Phase-Doppler interferometry with probe-to-droplet size ratios less than unity. I. Trajectory Errors

Peter A. Strakey, Douglas G. Talley, Subra V. Sankar, and Will D. Bachalo

Phase-Doppler interferometry in which a probe volume that is much smaller than the droplets being measured has been shown to work well when coupled with a phase-ratio and intensity-validation scheme that is capable of eliminating trajectory-dependent scattering errors. With ray-tracing and geometric-optics models, the type and magnitude of trajectory errors were demonstrated quantitatively through stochastic trajectory calculations. Measurements with monodispersed water droplet streams and glass beads were performed to validate the model calculations and to characterize the probe volume. Scattered-light intensity has also been shown to provide a robust means of determining the probe cross-sectional area, which is critical for making accurate mass flux measurements.

OCIS codes: 120.3180, 120.4640, 120.5050.

1. Introduction

Measurements of droplet size, velocity, and volume flux in optically dense sprays is an emerging and challenging field. One promising technique that is capable of measuring all these parameters is phase-Doppler interferometry (PDI). The PDI technique, which works well in low number density sprays (N less than 10^3 cm^{-3}) in a size range of 5–300 μm, is fraught with problems in dense, polydisperse sprays, for which the total number density can typically reach 10^5 cm^{-3}. The PDI technique is a single-particle counting method that relies on the fact that there is no more than one particle in the probe volume at any given time. As an example, for a log-normal distributed spray in the size range of 5–300 μm with a geometric standard deviation of 2.3 the number mean diameter D_{10} would be of the order of 10% of the maximum droplet size of 300 μm. Inasmuch as the droplet number density would decrease with increasing droplet size, the average droplet spacing for simple cubic packing would increase with increasing droplet size with an average spacing ($N^{-1/3} - D_{10}$) of the order of 170 μm.

High-pressure liquid rocket injectors produce a wide range of droplet sizes, depending on the injector flow rates, chamber pressure, and injector geometry (shear coaxial, swirl, impinging, etc.). In an effort to maintain high engine operating efficiency, liquid rocket injectors usually operate at very high flow rates, of the order of several kilograms per second, and high backpressure. This combination of high flow rate and high pressure results in high number densities of relatively large droplets. A shear coaxial injector that is currently being studied at the U.S. Air Force Research Laboratory AFRL uses water and nitrogen as simulants for liquid oxygen and gaseous hydrogen and has produced droplet sizes in the range of 2–200 μm with total number densities of ~10^5 cm^{-3}. The conventional PDI technique requires that the diameter of the probe volume be at least twice as large as the largest droplet size to be measured. This rule of thumb is designed to minimize trajectory-dependent scattering errors that occur when the droplet size becomes larger than the probe radius. The probe volume can be estimated by

$$V = \frac{\pi D_w{}^2 D_s}{4 \sin(\theta)}, \tag{1}$$

where D_w is the $1/e^2$ beam waist diameter, D_s is the apparent slit width, and θ is the angle of the receiver with respect to the laser beams. The apparent slit

P. A. Strakey (peter_strakey@ple.af.mil) and D. G. Talley are with the U.S. Air Force Research Laboratory, AFRL/PRSA, 10 East Saturn Boulevard, Edwards Air Force Base, California 93524. S. V. Sankar and W. D. Bachalo are consultants at 14660 Saltamontes Way, Los Altos Hills, California 94022.

Received 5 November 1999; revised manuscript received 4 April 2000.

width is equal to the slit width multiplied by the magnification factor of the receiving optics. For a scattering angle of 30°, a beam waist of 400 μm, and an apparent slit width of 200 μm, the probe volume is 5.0×10^{-5} cm^3. By treating the droplets as infinitesimally small, one can determine the probability of finding n particles within the probe volume by

$$P(n) = \frac{(VN)^n}{n!} e^{-(VN)}, \tag{2}$$

where V is the probe volume and N is the particle number density.[1] For the configuration listed above with $N = 10^5$ droplets/cm^3, the ratio of $P(2)/P(1) = 2.5$, which means that probability of finding two particles in the probe volume is 2.5 times the probability of finding one particle in the probe volume. Because the scattered-light intensity from a droplet is proportional to the square of the droplet diameter and the intensity distribution of the probe beams is Gaussian, the probe size for a given minimum signal detectability increases with increasing droplet size. In Eq. (1) the diameter of the probe volume is estimated to be D_w, which could better be described as an average probe volume diameter.

It is unclear how an instrument responds when several particles are simultaneously present in the probe volume. Sankar *et al*. have shown that a discrete Fourier-transform-based (DFT) signal processor can, in some instances, measure one of two particles that are simultaneously present in the probe volume.[1] The DFT signal processor cannot, however, account for the other particle(s) that are present in the probe volume. The result can be a severe underestimation of the particle number density and volume flux and a potential biasing in the particle size distribution.

There is a relatively small collection of published literature with respect to making phase-Doppler measurements when the probe-to-particle diameter ratio is small ($D_w/D < 1.0$).[2–6] Most of these studies are theoretical in nature, involving geometric optics or generalized Lorenz–Mie theory to calculate the far-field scattering for droplets that are comparable to or larger than the probe diameter. One problem has been referred to as trajectory-dependent scattering errors or trajectory ambiguities.[2–17] Hardalupas and Liu[2] presented a theoretical study in which they used a geometric-optics phase-Doppler response model to predict the resultant phase and intensity for various droplet trajectories through the probe volume for D_w/D ratios down to 0.35. They showed, for nonabsorbing droplets at various scattering angles, that significant sizing errors can occur for certain trajectories on the edge of the probe volume away from the receiver. They concluded that most of the sizing errors can be eliminated by an appropriate phase- and intensity-validation scheme. They also showed that forward scattering is preferable to side or backward scattering with respect to minimizing trajectory errors when one is sizing nonabsorbing droplets.

Haugen and co-workers[3] demonstrated in theory and through experimentation with a monodispersed droplet stream that trajectory errors can be eliminated with a three-detector system for a D_w/D ratio of 0.17 by use of a phase-ratio criterion between the two pairs of detectors. The technique was shown to work best when the detector separation ratio between detectors 1 and 2 and detectors 1 and 3 was a noninteger number with a fractional part close to 0.5, i.e., $S_{13}/S_{12} = 2.5$ or $S_{13}/S_{12} = 3.5$. The use of noninteger detector separations is discussed below.

Hadalupas and Taylor[4] proposed a phase-validation criterion to eliminate sizing errors caused by trajectory ambiguity, but their method requires that the maximum droplet size in a spray be known *a priori* and that the optical system be arranged such that the maximum measured phase that is due to refraction be less than the minimum phase that is due to reflection over the size range of interest. This method would be difficult to apply to a spray for which the investigator had no knowledge about the anticipated droplet size range.

Various researchers have proposed variations on the standard PDI technique that are designed to reduce or eliminate sizing errors. These techniques involve changing the orientation of the receiving optics with respect to the predominant flow direction as well as adding additional receiving optics. A review of these techniques and a discussion of some of the problems of variations of the standard PDI technique were presented by Sankar and Bachalo.[14] Their conclusion was that all the variations of the standard PDI technique introduced new problems that would have to be overcome to make any of the techniques feasible.

Sankar *et al*.[15] demonstrated through geometric-optics modeling and experimentation that significant sizing errors occur for certain droplet trajectories for D_w/D ratios less than ~2.9. They demonstrated that one can minimize trajectory errors by increasing the laser beam intersection angle; their experimental results have shown this to work quite well for D_w/D ratios down to 1.4.

Sankar and co-workers[16] also demonstrated that trajectory errors occur for droplet trajectories along the edge of the probe volume and are associated with a low scattering intensity, which can subsequently be used to identify and eliminate these erroneous measurements. There is no fundamental limit on the minimum D_w/D ratio for which this technique would work. Intensity validation is an attractive technique because most existing PDI systems already have the capability to measure peak scattering intensity and to reject measurements below a preset scattering intensity.

2. Trajectory Errors

For many spray applications involving nonabsorbing droplets, and for dense sprays in particular, the placement of the receiving optics in the refraction-dominated forward-scattering region ($25° < \theta < 45°$) is better than side scattering or backscattering because of its increased light-scattering intensity and,

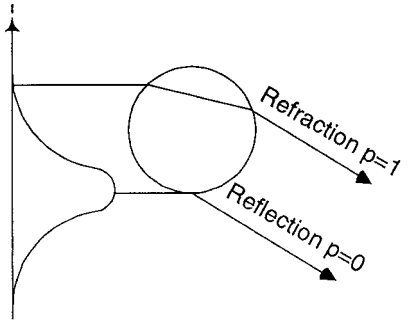

Fig. 1. Trajectory-dependent scattering.

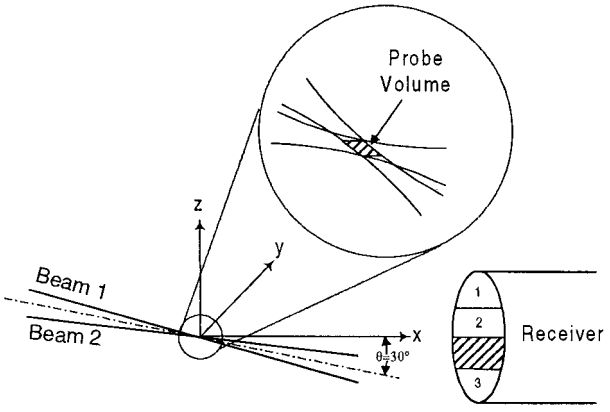

Fig. 2. Optical arrangement for modeling calculations.

thus, signal-to-noise ratio. One of the problems associated with reducing the size of the probe volume for this optical configuration is trajectory-dependent scattering, which is a result of the Gaussian nature of the laser beam waist and occurs when the probe-to-droplet diameter ratio, D_w/D, is less than approximately 2.9.[5] Droplets of this size that pass through the edge of the probe volume, as shown in Fig. 1, have a significant reflection-scattering component, which can result in the droplet's being erroneously sized as either a smaller or a larger droplet, depending on the optical configuration and droplet size. This phenomenon was demonstrated previously with both theoretical light-scattering calculations and experimentation.[16] It has also been shown that these reflection-tainted trajectories can be identified by their relatively low light-scattering intensities.[16]

One of the goals of this investigation is to demonstrate with both theoretical calculations and experimentation that trajectory-dependent errors for nonabsorbing droplets in the forward-scattering regime can be eliminated with an appropriate phase-ratio and intensity-validation scheme. The ability to eliminate trajectory-dependent scattering errors allows for making the beam waist diameter and hence the probe volume much smaller than the largest droplet size to be measured, thereby permitting the application of PDI in sprays with significantly higher number densities than was previously possible.

3. Modeling and Experimental Results and Discussion

A. Geometric-Optics Modeling

We used a previously developed phase-Doppler response model[7] to study the effect of droplet trajectory on phase response and scattering intensity. The model is a geometric-optics-based scattering model that accounts for the Gaussian nature of the illuminating probe beams by integrating the appropriate scattering functions over the surface of the receiving lens. The model accounts for external surface reflection ($p = 0$) and refraction ($p = 1$) and the first four modes of internal reflection ($p = 2$–5). The model calculates the resultant phase and intensity for each detector in the receiver. The geometric-optics model has been shown to yield excellent agreement with Lorenz–Mie theory for droplet sizes larger than the wavelength of light when the scattered phase and intensity are integrated over a typical ($f = 5.0$) receiver lens.[14] The model will not be discussed further here; the reader is referred to the published description of the model.[7]

A schematic of the optical orientation is presented in Fig. 2. The receiver lies in the x–y light-scattering plane at 30° with respect to the beam propagation direction. The trajectory coordinate, η, is defined as y/D_w, where y is the distance from the center of the probe volume in the light-scattering plane normal to the beam propagation direction and D_w is the $1/e^2$ beam waist diameter. For the calculations presented here, all trajectories were normal to the light-scattering plane in the negative z direction. Negative values of η would correspond to trajectories on the side of the probe farthest from the receiver. The calculations were performed for the optical configuration listed under case 1 in Table 1. Figures 3(a) and 3(b) are plots of φ_{12} and φ_{13}, whereas Figs. 3(c) and 3(d) are plots of calculated scattered-light intensity normalized by the maximum intensity, the calculated droplet diameter normalized by the actual

Table 1. Values of Parameters in Configurations for Experiments and Model Calculations

Optical Parameter	Case 1	Case 2
Beam separation (mm)	21	21
Transmitter focal length (mm)	470	470
Receiver focal length (mm)	500	500
Scattering angle (deg)	30	30
Initial beam diameter (mm)	10.0	10.0
$1/e^2$ beam waist diameter (μm)	60	60
Slit width (μm)	50	50
Receiver magnification	2.0	2.0
Receiver lens diameter (mm)	105	105
Laser wavelength (nm)	514.5	514.5
Fringe spacing (μm)	11.52	11.52
S_{12} (mm)	23.34	25.0
S_{13} (mm)	69.00	65.0
S_{13}/S_{12} (mm)	2.96	2.6
Sample rate (MHz)	160	160
Sample size	64	64

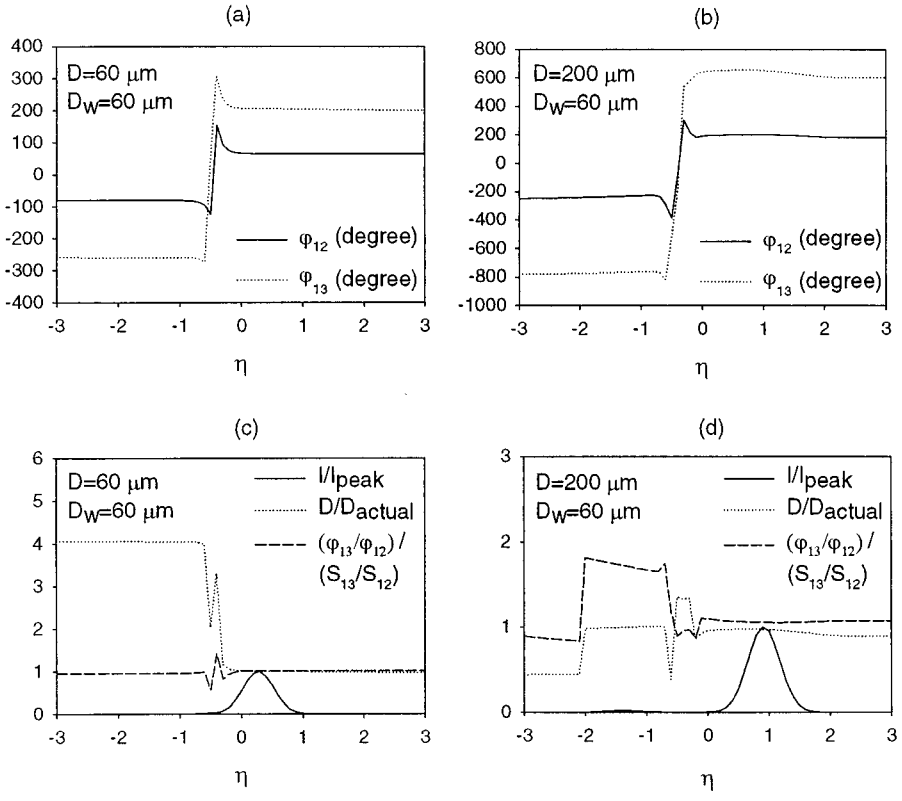

Fig. 3. (a), (b) Model calculations of φ_{12} and φ_{13} and (c), (d) normalized scattered-light intensity, diameter, and phase ratio for droplet diameters of 60 μm and 200 μm. Water droplets; optical arrangement of case 1, Table 1.

diameter, and the calculated phase ratio between detector pairs 1 and 3 and 1 and 2 normalized by the detector separation ratio (2.96). These calculations are shown as a function of η for water droplet diameters of 60 and 200 μm. In these plots the calculated diameter is based on the phase response of detector pairs 1 and 3. Because the instrument is capable of measuring only positive phase values, the calculated phase values in Figs. 3(c) and 3(d) are subsequently reported as being positive. For example, a 60-μm droplet at $\eta = -2.0$ results in phase values of $\varphi_{12} = -81°$ and of $\varphi_{13} = -260°$ owing to reflection-dominated scattered light. The instrument actually measures φ_{12} as $-81° + 360° = 279°$. Similarly, $\varphi_{13} = -260° + 360° = 100°$. Inasmuch as φ_{13} is actually multivalued over the detectable size range, the correct φ_{13} is calculated by use of φ_{12} to determine which cycle φ_{13} is in. φ_{13} is calculated according to the following equation:

$$\varphi_{13} = \varphi_{13} + \text{Trunc}\left(\frac{\varphi_{12} S_{13}}{360° S_{12}}\right) \times 360°, \qquad (3)$$

where Trunc is a truncation function equal to the integer portion of the division.

For a 60-μm droplet [Figs. 3(a) and 3(c)], for η greater than -0.3, refraction dominates the scattered-light signal (positive phase values) and the normalized diameter and phase ratio are equal to 1.0. For η less than -0.3, reflection begins to contribute significantly to the scattered-light signal, resulting in negative phase values and a measured diameter of 240 μm, which is much larger than the actual diameter of 60 μm. It is interesting to note that the normalized phase ratio in this region is still equal to 1, indicating that most of these measurements would pass the phase-ratio validation criterion that requires that $\varphi_{13}/\varphi_{12} = S_{13}/S_{12}$ within a tolerance band of ±10%. This is a problem unique to instruments with a detector separation ratio equal to an integer number. For such a detector configuration, any reflectively dominated trajectory will pass the phase-ratio validation criterion. For instance, for a 60-μm droplet at $\eta = -1.0$, φ_{12} is calculated to be $-81.7°$ and $\varphi_{13} = -260.0°$. The instrument would measure φ_{12} as $-81.7° + 360.0° = 278.3°$. Similarly, $\varphi_{13} = -260.0° + 360.0° = 100.0°$. Using Eq. (3), we find that φ_{13} is in the third cycle; therefore $\varphi_{13} = 100.0° + 720.0° = 820.0°$. The resultant phase ratio, $\varphi_{13}/\varphi_{12} = 2.95$, is almost exactly equal to the detector separation ratio S_{13}/S_{12} of 2.96.

The problems associated with using integer values of the detector separation ratio have been demonstrated in theory and can be overcome by use of a noninteger detector separation ratio such as 2.5.[3] Also, note from Fig. 3(c) that the normalized phase ratio in the region of $-0.6 < \eta < -0.2$ is not equal to 1.0 and would probably be rejected by the instrument, even with an integer detector separation ratio. The scattered light for these trajectories is a mix of refraction and reflection, and thus the phase is a complicated result of the coherent interaction between these two scattering modes that results in phase ratios' deviating from 1.0.

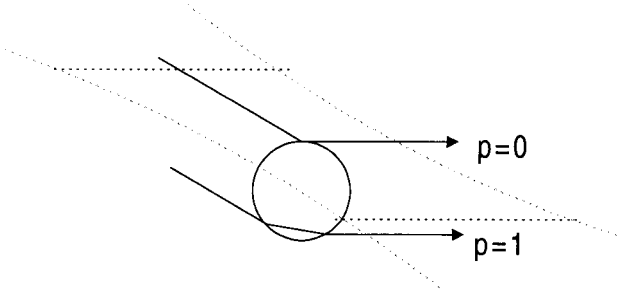

Fig. 4. Illustration of the slit effect. Lighter dashed lines, beam edge; darker dashed lines, slit edge. Ray paths of reflection ($p = 0$) and refraction ($p = 1$) are shown.

Figures 3(b) and 3(d) show similar results for the 200-μm droplets. Figure 3(d) shows that for a 200-μm droplet the refractively dominated scattered light has a peak intensity near $\eta = 1.0$, whereas the reflectively dominated light is centered at approximately $\eta = -1.5$. This is so because refraction and reflection originate from opposite sides of the droplet, as illustrated in Fig. 1. For the 200-μm droplets [Fig. 3(d)], note that the normalized phase ratio and the normalized calculated droplet size do deviate from 1 throughout the beam waist. This is so because of the decrease in signal visibility of the refracted-light signal for the larger droplet size. The signal visibility is defined as the relative amplitude modulation of the scattered-light signal as a droplet passes through the probe volume.

Figures 3(a)–3(d) show that severe sizing errors can occur for certain trajectories through the probe volume and that most of these erroneous measurements will pass the phase-ratio validation criterion of a three-detector instrument when the detector separation ratio is close to an integer number. Figure 3 does not, however, reveal the magnitude of the problem, which depends on the relative probability of any given trajectory and the minimum detectable signal that will trigger the burst detector. Also, another type of measurement error, sometimes referred to as the slit effect, can cause erroneous measurements.[17] The slit effect occurs for certain particle trajectories when the spatial filter in the receiving optics, referred to as the slit, blocks the refractively scattered light signal but passes the reflectively scattered light signal, resulting in a measurement error similar to that shown in Fig. 3. Figure 4 illustrates the slit effect.

B. Experimental System

The PDI system used in this study was a commercially available system manufactured by Aerometrics, Inc. The optical configuration is described in Table 1 (case 1). The transmitter produced a beam waist of 352 μm with a 500-mm focusing lens. To reduce the beam waist diameter we constructed a beam expander that used a negative achromatic lens ($f_1 = -12$ mm) and a positive achromatic lens ($f_2 = 60$ mm) to expand and recollimate the beams inside the transmitter from an initial diameter of 2.0 mm to a final diameter of 10.0 mm. We characterized the resultant beam waist by placing a microscope objective at the beam crossover point and projecting the beam waist onto a rotating white target. The rotation of the target served to reduce the speckle pattern formed by the coherent laser. The beam waist was then imaged with a CCD camera and recorded with a frame grabber. The $1/e^2$ beam waist, which was close to Gaussian in shape, was measured to be 60 μm in diameter. The standard receiver slit, which was 100 μm, was replaced with a 50-μm slit to reduce the probe volume further. Because of the factor-of-2 magnification in the receiving optics, the apparent slit width was 100 μm.

The signal processor was a one-bit DFT-based processor with peak detection capability. The peak detector ensures that the sampled data set used for calculation of frequency and phase is centered about the peak of the Doppler burst signal where the signal-to-noise ratio is maximized. The peak detector is also employed in the measurement of the signal amplitude, or intensity. The signal processor uses a combination of analog and DFT-based burst-detection schemes that trigger the peak detector only when the signal is of sufficient amplitude and coherency.

C. Stochastic Ray-Trace Modeling

To investigate the combined effects of trajectory error and the slit effect we used a ray-tracing algorithm to predict the relative intensity of refractively and reflectively scattered light as a function of droplet size and trajectory in a two-dimensional probe volume defined by the beam waist and the receiver slit. Droplet trajectories, as defined by the x and y coordinates, were chosen by a random-number generator and encompassed an area much larger than the beam waist and slit width. The resultant scattered-light intensity was calculated and compared with a minimum detectable signal level.

The minimum detectable raw signal for the signal processor was determined by experimentation with a 16-point DFT burst detector to be approximately $1/500^{\text{th}}$ (1 mV) of the saturation signal. The threshold setting was the minimum amplitude of the high-pass filtered, log amplified signal before triggering can occur. A setting of 3 mV was close to the minimum usable level before triggering on background noise would occur.

For the droplets with calculated scattered-light intensities greater than the minimum detectable intensity, significant sizing errors were determined to occur when the intensity of the reflectively scattered-light component was greater than 50% of the total scattered-light intensity. This criterion was determined through geometric-optics calculations similar to those in Fig. 3. This type of ray-tracing calculation can determine which trajectories will result in sizing errors but provides no information as to the magnitude of the errors. For each droplet size and optical configuration, 25,000 random trajectories were selected, and the fraction of measurements

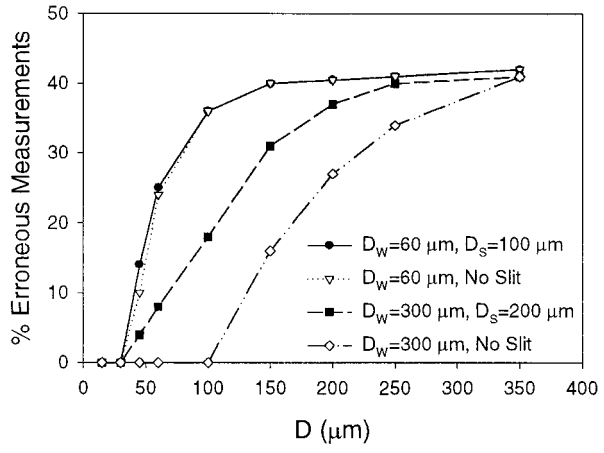

Fig. 5. Fraction of measurements with significant sizing errors versus droplet size for 60- and 300-μm probe diameters with and without the slit effect.

dominated by reflective contributions was tabulated. Figure 5 shows the fraction of measurements in which sizing errors would occur. Calculations were performed for beam waist diameters of 60 and 300 μm with and without the receiver slit in place. For the 300-μm probe diameter the relative number of erroneous measurements increases with droplet size and also increases when the receiver slit is accounted for. The 60-μm beam diameter reveals an increase in erroneous measurements, in comparison with those for the 300-μm probe, for any given droplet size. This result is due to an increased reflective contribution to the scattered-light signals for the smaller beam waist/droplet size ratio. With the 60-μm beam waist the receiver slit appears to have no effect; in other words, the same errors would occur even without the slit blocking the refractively scattered light for certain trajectories. The reason for this is that, with a beam waist smaller than the apparent slit width, errors occur only for droplet trajectories on the far side of the beam waist with respect to the receiver. For these trajectories, sizing errors occur as a result of the Gaussian intensity distribution of the probe beams, and the introduction of the receiver slit does not serve to aggravate this problem further.

Figure 5 shows that an alarming number of sizing errors can occur for droplet sizes much larger than the beam waist. For dense spray applications, when the beam waist is made much smaller than the largest droplets that are being measured, the largest number of trajectory errors will occur in the droplet size classes with the highest number density. For a beam waist of 60 μm and a maximum droplet size of ~300 μm, peak number densities in a typical dense spray might occur in the 50–100-μm range. It is these droplets' being erroneously measured as much larger droplets that will statistically contribute the most to errors in the higher-moment diameters such as D_{30} and D_{32} and in the measured mass flux, which tends to scale with D_{30}.

D. Stochastic Geometric-Optics Modeling and Experimentation

1. Small Droplets Measured As Larger Droplets

Knowing that the receiver slit does not contribute to sizing errors for beam waists smaller than the apparent slit width, we can now use the geometric-optics model, which does not account for slit effects, to estimate more quantitatively the magnitude of trajectory-dependent scattering errors. An approach similar to that described above for the ray-tracing calculations was taken. A random-number generator randomly selected trajectories (with respect to the y direction) normal to the scattering plane, and the resultant phase and intensity were calculated. Negative phases were then calculated as being positive, and droplet sizes were calculated with a linear refractive phase response curve. The calculated droplet sizes were grouped in size bins to yield a histogram of counts verses droplet size similarly to the way in which commercial instruments work experimentally. All calculations and experiments were performed with water droplets with refractive indices of $1.33–0.0i$. The optical configuration was the same as in case 1 of Table 1.

To verify the model calculations quantitatively, we conducted several experiments with an acoustically driven monodispersed droplet generator. A laminar stream of water issuing from a small orifice was perturbed by a piezoelectric crystal mounted upon the droplet generator, which produced a steady stream of droplets traveling at 13 m/s at a rate of $\sim 10^4$ droplets/s. For each droplet size studied, 30,000 data points were collected while the droplet generator was traversed, by hand, throughout the probe volume over a period of ~30 s. The manual traversing produced pseudorandom trajectories through the probe volume. In an effort to verify the randomness of the trajectories, we repeated each 30,000 point data set twice and calculated the Sauter mean diameter, D_{32}, for each run. The standard deviation normalized by the mean D_{32} for the three runs was of the order of 11% for each droplet size studied. Although there was some variation from run to run, each data set does represent a random selection of trajectories fairly well.

Figure 6 contains a series of histograms of calculated diameter from the geometric-optics model and measured diameter from the monodispersed droplet experiments for random trajectories through the probe volume for a droplet diameter of 57 μm. The optical configuration was that of case 1 of Table 1. Figures 6(a) show the model and experimental results without the use of a phase-ratio criterion. The model shows excellent agreement with the experimental results not only for the location of the erroneous peak in the histograms, which occurs at 250 μm, but also in the relative number of trajectory errors in comparison with the correctly measured droplets at 57 μm. For the experimental histogram in Fig. 6(a) the measured D_{32} was 224 μm, which was dominated by the relatively few falsely measured

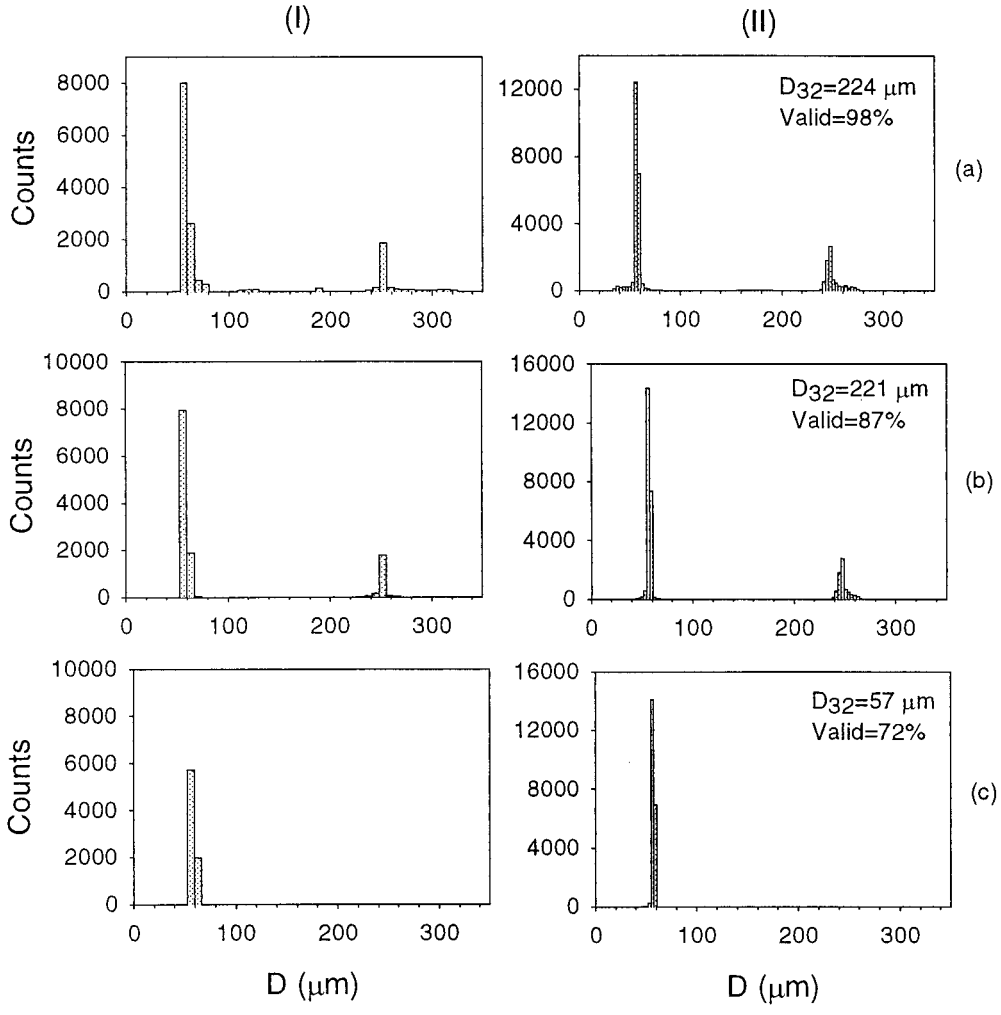

Fig. 6. Histograms of (I) calculated droplet size and (II) measured droplet size for 57-μm droplets on random trajectories (a) without a phase-ratio criterion, (b) with a ±10% phase-ratio criterion, and (c) with a ±10% phase-ratio and a 10:1 intensity-validation criterion. Water droplets; optical configuration from case 1, Table 1.

large droplets. This large measurement error demonstrates the need to reject the trajectory-dependent errors.

Figure 6(b) contains histograms of the same data set presented in Fig. 6(a) but with the phase-ratio criterion applied. The phase-ratio criterion requires that $(\varphi_{13}/\varphi_{12}) = (S_{13}/S_{12})$ to within ±10%. Both the model calculations and the experimental data confirm that almost all the erroneous measurements pass the phase-ratio validation criterion, which is a result of the near integer detector separation ratio, S_{13}/S_{12}, of 2.96.

Figure 6(c) shows the same data set as Fig. 6(b), after a 10:1 intensity-validation criterion is applied. The 10:1 intensity-validation scheme rejects measurements with a scattering intensity less than 10% of the maximum scattering intensity in each size class. The intensity-validation scheme depends not on the absolute scattering intensity but only on the ratio of the measured scattering intensity to the maximum measured scattering intensity within each size group. This validation procedure is general with regard to the PDI technique and can be used with any instrument that is capable of measuring the peak scattering intensity of the raw Doppler burst signal. Both the model and the experiment show that all the erroneous measurements are rejected.

Figure 7 shows model calculations and experimental results for a 98-μm droplet diameter. The data are again presented without the phase-ratio validation criterion [Fig. 7(a)], with the phase-ratio criterion applied [Fig. 7(b)], and with the 10:1 intensity-validation criterion applied [Fig. 7(c)]. The results are the same as for the 57-μm droplets, confirming that the phase-ratio criterion accepts most of the erroneous measurements at 200 μm but that all of them can be rejected with a 10:1 intensity-validation criterion.

Model calculations were performed over a wide range of droplet sizes from 10 to 350 μm in diameter. The model has shown that significant sizing errors occur for D_w/D ratios less than ~5.0 for the optical configuration of case 1, Table 1. Because of minimum detectability limits of the instrument, the practical maximum D_w/D at which sizing errors occur would be ~2.0. The model has also shown that a 10:1 intensity-validation criterion is sufficient to reject any trajectory-dependent scattering error that would result in a droplet's showing up as a larger droplet. In most sprays this will be the statistically

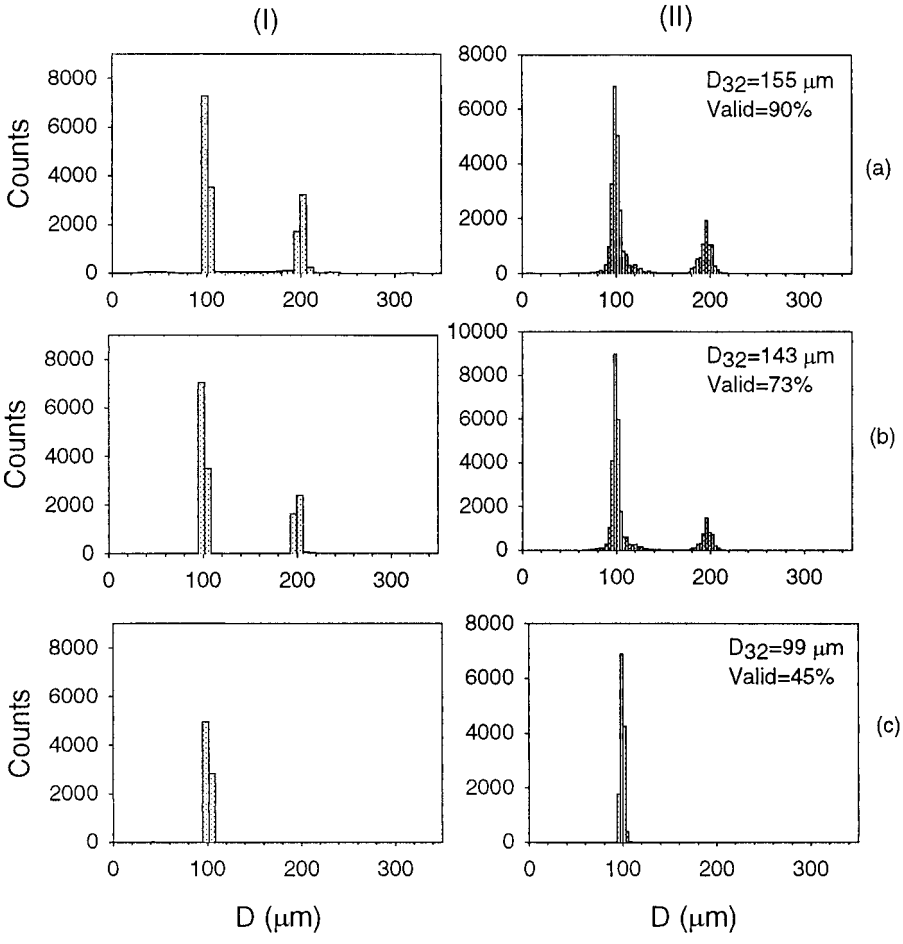

Fig. 7. Histograms of (I) calculated droplet size and (II) measured droplet size for 98-μm droplets on random trajectories (a) without a phase-ratio criterion, (b) with a ±10% phase-ratio criterion and (c) with a ±10% phase-ratio and a 10:1 intensity-validation criterion. Water droplets; optical configuration from case 1, Table 1.

dominant sizing error. Large droplets passing along the far side of the probe volume can, however, be misinterpreted as smaller droplets with corresponding low scattering intensity. The intensity-validation criterion will not be able to reject these types of error.

2. Large Droplets Measured As Smaller Droplets

To reject errors associated with large droplets being measured as much smaller droplets, a phase-ratio validation criterion can be applied with a noninteger detector separation, as demonstrated by Haugen *et al.*[3] In theory, a noninteger phase-validation criterion should also be able to reject small droplets that show up as much larger droplets. An experiment was conducted in which we changed detector separations S_{12} and S_{13} by placing a mask in front of the receiver lens, effectively blocking off some portion of each detector. This resulted in a separation of detectors 1 and 2 of 25.0 mm and a separation of detectors 1 and 3 of 65.0 mm (case 2, Table 1). The detector separation ratio was 2.6. Experiments were repeated with the pseudorandom monodispersed droplet stream for droplet diameters of 61, 102, and 250 μm.

Figure 8 contains histograms for the 250-μm droplet size. For this relatively large droplet size, a reflective error results in the droplet being measured as a much smaller droplet of 60-μm diameter. The broadness of the two peaks in Fig. 8(a) is a result of some degree of nonsphericity for the relatively large droplet size of 250 μm, which we verified by imaging the droplet stream with a CCD camera and a strobe light. Applying the phase-ratio criterion of ±10% to the data in Fig. 8(a) results in the histogram shown in Fig. 8(b), which shows a great decrease in the number of erroneous measurements at the 60 μm peak. There are, however, some errors that pass the validation criterion, but, statistically, the overall error in a typical spray would be small, because the number density of real droplets in the 60-μm size range would be much larger than the number density at 250 μm.

For the experiments with the 61-μm droplets we reduced the number of counts at the reflection peaks at 70 and 270 μm by almost a factor of 8 with the noninteger detector separation and phase-ratio validation criterion of ±10%, but enough passed the criterion to produce a D_{32} of 101 μm. Figure 9 shows the volume distribution, which is the number of counts multiplied by D^3 for each size class, with and without the phase-ratio validation criterion. The volume distributions are used to illustrate the significant effect of a very small number of very large droplets. Similar results were obtained with the 102-μm

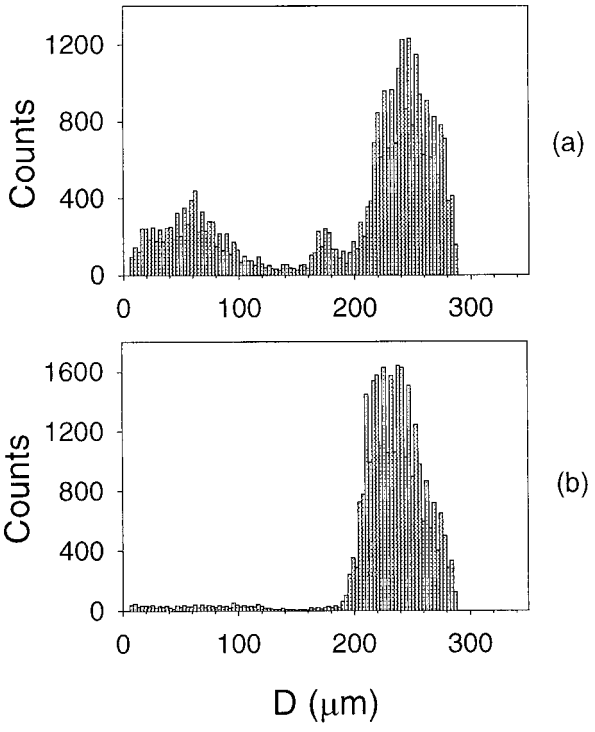

Fig. 8. Histograms of experimentally measured counts for 250 μm water droplets on random trajectories (a) without a phase-ratio criterion and (b) with a phase-ratio criterion. Noninteger detector separation; optical configuration from case 2, Table 1.

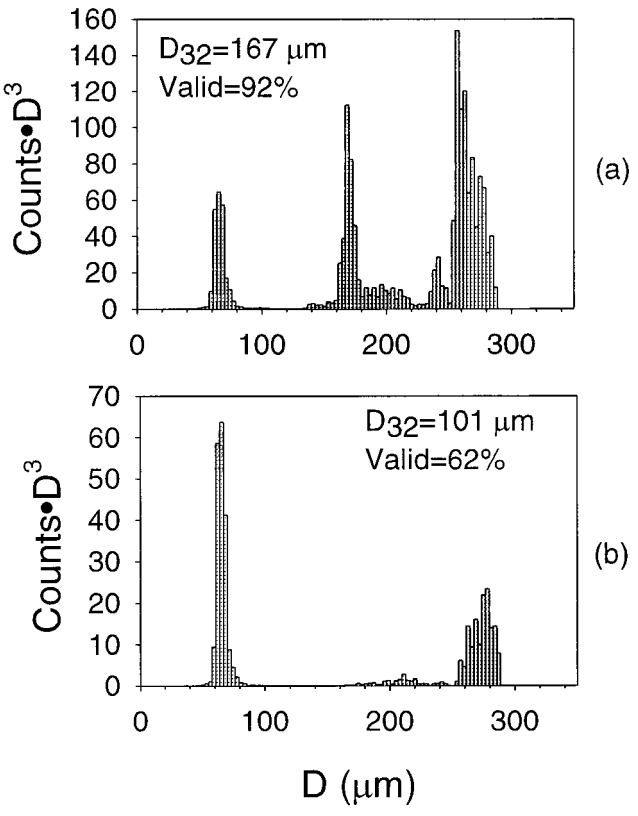

Fig. 9. Experimentally measured relative volume distributions (counts $\times D^3$) for 61-μm water droplets on random trajectories (a) without a phase-ratio criterion and (b) with a phase-ratio criterion. Noninteger detector separation; optical configuration from case 2, Table 1.

droplets. The small number of measurements that pass the phase-ratio validation criterion could be the result of some small amount of noise-related error in the phase measurement caused by the relatively short transit times. These results demonstrate that using a noninteger detector separation can eliminate most, but not all, trajectory errors. Significant overestimation of the higher-moment diameters can still occur when large number densities of droplets with diameters similar to the probe diameter are present in a spray.

Both the calculations and the experiments indicate that trajectory-dependent phase errors occur only at scattering intensities well below a scattering intensity that is 10% of the maximum intensity for each droplet size. Similar results were published previously and demonstrated that probe diameters much smaller than the droplets that are being measured can provide accurate droplet size measurements when a phase ratio with a noninteger detector separation ratio and scattering intensity are used as criteria to reject trajectory-dependent scattering errors.

E. Detailed Probe Volume Characterization

The model calculations and experimental results presented herein have shown that, even for a beam waist much smaller than the droplet that is being measured, accurate size measurements can be made within a 10:1 intensity range. These results do not, however, necessarily show that droplets within the 10:1 intensity range are being validated by the instrument. Also, the effective size of the probe cross-sectional area, which can be ascertained by the measured scattered-light intensity, has not been shown necessarily to be accurate. For a Gaussian beam waist, the probe cross-sectional area is a function of the beam waist diameter at the 10:1 lower intensity cutoff and the apparent slit width and scattering angle according to

$$A = \frac{D_{w10\%} D_s}{\sin(\theta)}. \tag{4}$$

To characterize the probe volume it was necessary to traverse the probe volume in both the x and the y directions with a stream of droplets in which the absolute droplet positions within the probe volume were known. It was determined that completely mapping the probe volume would require several hours of data collection and that the monodispersed droplet generator was not capable of maintaining a sufficiently steady stream of droplets for this period of time. It was found that a similar type of experiment could be conducted with a glass bead mounted upon 126-μm steel wire, which was in turn mounted upon a rotating disk. The rotating disk would swing the glass bead through the probe volume at a velocity of 16 m/s. This arrangement was found to produce

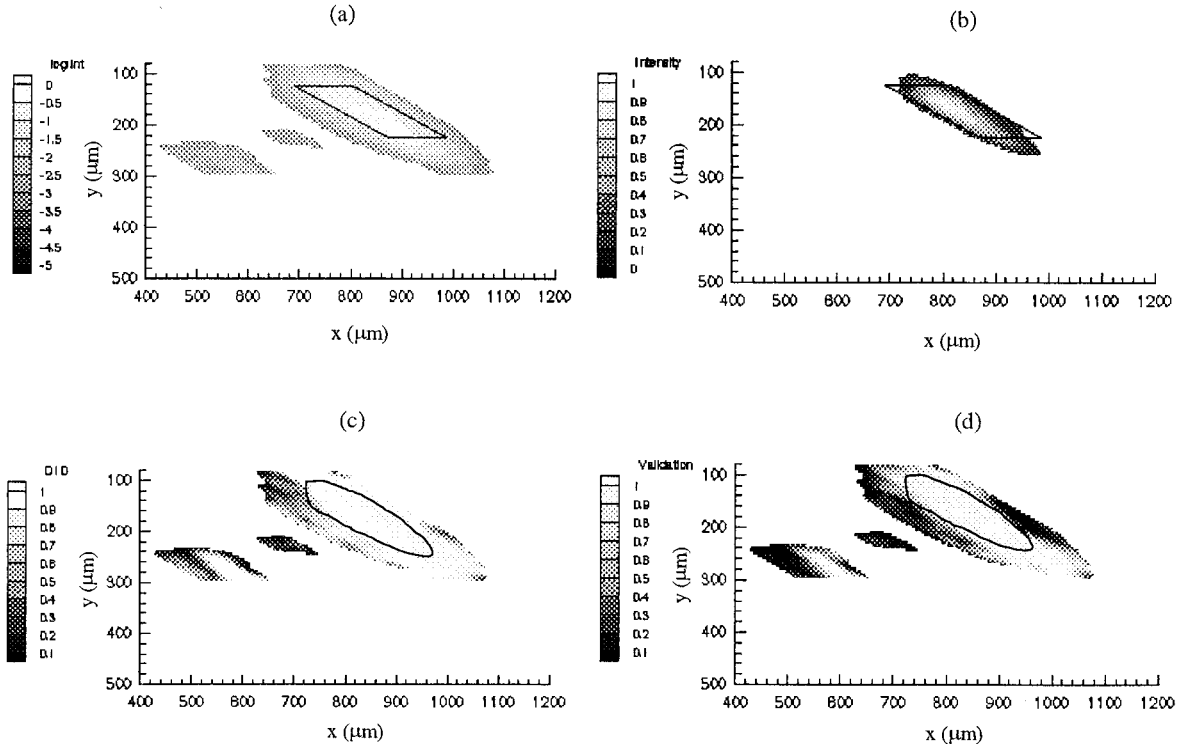

Fig. 10. Contour plots of measured (a) log of the normalized intensity, (b) linear normalized intensity over a 10:1 range, (c) normalized D_{10}, and (d) normalized validation rate. Parallelograms; assumed probe cross sections. 330-μm glass bead; optical configuration from case 1, Table 1.

steady and repeatable results. The glass bead was examined under a microscope to ensure that it was free from surface defects and inclusions. Glass has a refractive index of 1.51 in air, which yielded a maximum measurable size of 370 μm with the optical configuration listed in Table 1, case 1.

The setup was mounted upon a three-dimensional translating stage, which allowed the bead to traverse through the probe volume with a positioning accuracy of 1 μm. The bead traversed in the x direction, toward the receiver, in 20-μm steps; 300 measurements were collected at each spatial location. The bead then traversed along the direction of the beams in 50-μm steps. The resultant data provided a two-dimensional map of measured bead size, scattering intensity, and validation rate across the entire probe cross-sectional area. Each data set, which comprised approximately 120 data points, was interpolated to allow contour plots to be presented.

Figure 10 contains contour plots of the log of the intensity, the intensity within a 10:1 range, the measured D_{10}, and the instrument validation rate. In each of the plots the beams originate from the upper left hand corner and the receiver is located at the right. The coordinate positions are relative to the initial bead starting position. Data are shown everywhere that an instrument trigger was obtained. Figure 10(a) shows the logarithm of the normalized intensity distribution for a 330-μm glass bead. The intensity was normalized by the maximum scattering intensity. Note the island of reflectively scattered light centered at $x = 530$ μm, which is a factor of 40 less intense than the refractively scattered light. The two scattered-light modes are separated in space because the refractively scattered light and the reflectively scattered light originate from opposite sides of the bead. For the large bead size studied here, there are trajectories between the two modes ($p = 0$ and $p = 1$) that result in no detectable light's reaching the receiver. These results agree well with the model, which shows that the reflectively scattering trajectories are completely separated spatially from the refractive trajectories for large droplets. Also shown in Fig. 10(a) is the assumed probe volume (parallelogram), which is 64 μm in width with a 100-μm apparent slit length. Without an intensity-based validation criterion, the effective probe cross-sectional area, as determined by instrument triggering, would be much greater than the assumed area.

Figure 10(b) shows the linear normalized intensity distribution over a 10:1 intensity range. Normally to the beam propagation direction the measured beam diameter is very close to the assumed diameter of 64 μm. The length of the probe volume (in the y direction) as defined by a 10:1 intensity range was found to be ~125 μm. The fact that the measured slit width is larger than the physical slit width of 100 μm can be attributed to the finite interrogation spot size on the droplet surface, which yields an average scattering intensity over this region. The effective slit width is also increased by the resolution of the

receiving optics that results in a blur spot of 15 μm. The blur spot and the finite interrogation spot size tend to spread the intensity distribution over a larger area.

Figure 10(c) is a contour plot of the measured D_{10} normalized by the actual bead diameter of 330 μm. Also shown is the probe volume as defined by a 10:1 intensity validation criteria. Within the probe volume, the measured D_{10} is very close to the actual bead diameter. Outside the 10:1 probe volume, significant sizing errors occur, with the 330-μm glass beam being measured as small as 20 μm for certain trajectories. Figure 10(d) shows the validation rate normalized by the maximum, or ideal, validation rate of 100%. Within the 10:1 probe volume, the validation rates are close to 100%, except at the edges where the validation rates begin to drop off, with most of the rejections being due either to the phase-ratio criterion or to the bead's being measured as a diameter outside the measurable range.

These measurements show that, even for a bead diameter 5.5 times larger than the $1/e^2$ beam diameter, accurate sizing is possible within a 10:1 intensity range. The diameter of the probe, as defined by a scattering intensity of 10% of the maximum intensity, is close to the assumed diameter of 64 μm. The effective apparent slit width was found to be ~25% larger than the assumed width, which could easily be accounted for by assumption of a larger slit width. Similar results were obtained with a 100-μm glass bead, which showed that the effective slit width within the 10:1 intensity range was ~20% larger than the physical slit width.

4. Conclusions

The use of small probe-to-particle diameter ratios in PDI has been shown to produce accurate droplet size measurements in a combined phase- and intensity-validation scheme. Without these validation criteria serious overestimations of the higher-moment diameters can occur as a result of droplets being erroneously measured as much larger droplets. It has also been shown that a phase-validation criterion that uses integer values of the detector separation ratio will validate most of the trajectory errors. A noninteger detector separation ratio has been demonstrated to reject the erroneous reporting of large droplets as much smaller droplets. The phase-validation criterion does, however, still validate the measurement of some small droplets as much larger droplets. The 10:1 intensity-validation criterion does reject these errors and provide a robust and simple method for determining the probe cross-sectional area, which greatly affects mass flux measurements. The use of small probe volumes can greatly improve measurement reliability in dense sprays for which multiple particle occurrences in the probe volume will affect the measurement.

Appendix A. Nomenclature

A	Probe cross-sectional area (μm^2)
D	Droplet diameter (μm)
D_s	Apparent slit width (μm)
D_w	$1/e^2$ beam waist diameter (μm)
$D_{w10\%}$	Probe diameter at 10% of I_{max} (μm)
D_{10}	Number mean diameter (μm)
D_{32}	Sauter mean diameter (μm)
N	Droplet dumber density (cm^{-3})
n	Number of droplets in probe volume
S	Detector separation (mm)
φ	Phase difference (deg)
η	Trajectory coordinate
θ	Scattering angle (deg)
Subscript 12	Detectors 1 and 2
Subscript 13	Detectors 1 and 3

References

1. S. V. Sankar, D. H. Buermann, A. S. Inenaga, K. M. Ibrahim, and W. D. Bachalo, "Coherent scattering in phase Doppler interferometry: response of frequency domain processors," presented at the Seventh International Symposium on Applications of Laser Techniques to Fluid Mechanics, Lisbon, Portugal, 11–14 July 1994.
2. Y. Hardalupus and C. H. Liu, "Implications of the Gaussian intensity distribution of laser beams on the performance of the phase Doppler technique. Sizing uncertainties," Prog. Energy Combust. Sci. **23,** 41–63 (1997).
3. P. Haugen, E. I. Hayes, and H.-H. von Benzon, "Size and velocity measurements of large drops in air and in a liquid–liquid two-phase flow by the phase-Doppler technique," Part. Part. Syst. Charact. **11,** 63–72 (1994).
4. Y. Hardalupas and A. M. K. P. Taylor, "Phase validation criteria of size measurements for the phase Doppler technique," Exp. Fluids **17,** 253–358 (1994).
5. P. A. Strakey, D. G. Talley, W. D. Bachalo, and S. V. Sankar, "The use of small probe volumes with phase Doppler interferometry," presented at the Eleventh Annual Conference on Liquid Atomization and Spray Systems, Sacramento, Calif., 17–20 May 1998.
6. P. A. Strakey, D. G. Talley, and W. D. Bachalo, "Phase Doppler measurements in dense sprays," presented at the Eleventh Annual Conference on Liquid Atomization and Spray Systems, Sacramento, Calif., 17–20 May 1998.
7. S. V. Sankar and W. D. Bachalo, "Response characteristics of the phase Doppler particle analyzer for sizing spherical particles larger than the light wavelength," Appl. Opt. **30,** 1487–1496 (1991).
8. H. Qui and C. T. Hsu, "Method of phase-Doppler anemometry free from the measurement-volume defect," Appl. Opt. **38,** 2737–2742 (1999).
9. G. Grehan, G. Gouesbet, A. Naqwi, and F. Durst, "Trajectory ambiguities in phase Doppler systems: study of a near-forward and near-backward geometry," Part. Part. Syst. Charact. **11,** 133–144 (1994).
10. A. Naqwi, F. Durst, and X.-Z. Liu, "An extended phase-Doppler system for characterization of multiphase flows," presented at the Fifth International Symposium on Applications of Laser Techniques to Fluid Mechanics, Lisbon, Portugal, July 1990.
11. G. Grehan, G. Gouesbet, A. Naqwi, and F. Durst, "Trajectory ambiguities in phase Doppler systems: use of polarizers and additional detectors to suppress the effect," presented at the Sixth International Symposium on Applications of Laser Techniques to Fluid Mechanics, Lisbon, Portugal, 20–24 July 1992.
12. Y. Aizu, M. Ziema, X. Liu, S. Hohmann and F. Durst, "PDA

system without Gaussian beam defects," presented at the Third International Congress on Optical Particle Sizing, Yokohama, Japan, August 1993.
13. C. Tropea, T.-H. Xu, F. Onofri, G. Grehan, and P. Haugen, "Dual mode phase Doppler anemometry," presented at the Seventh International Symposium on Applications of Laser Techniques to Fluid Mechanics, Lisbon, Portugal, 11–14 July 1994.
14. S. V. Sankar and W. D. Bachalo, "Performance analysis of various phase Doppler systems," presented at the Fourth International Congress on Optical Particle Sizing, Nurnberg, Germany, 21–23 March 1995.
15. S. V. Sankar, A. S. Inenaga, and W. D. Bachalo, "Trajectory dependent scattering in phase Doppler interferometry: minimizing and eliminating sizing errors," presented at the Sixth International Symposium on Applications of Laser Techniques to Fluid Mechanics, Lisbon, Portugal, 20–24 July 1992.
16. S. V. Sankar, W. D. Bachalo, and D. A. Robart, "An adaptive intensity validation technique for minimizing trajectory dependent scattering errors in phase Doppler interferometry," presented at the Fourth International Congress on Optical Particle Sizing, Nurnberg, Germany, 21–23 March 1995.
17. T.-H. Xu and C. Tropea, "Improving the performance of two-component phase Doppler anemometers," Meas. Sci. Technol. **5,** 969–975 (1994).